Research Square

Preprints are preliminary reports that have not undergone peer review.
They should not be considered conclusive, used to inform clinical practice,
or referenced by the media as validated information.

Toward a Measurement of Stellar Oxygen Formation with the Warsaw Active Target TPC Operating in Gamma Beams

Kristian Haverson

k.haverson@shu.ac.uk

Sheffield Hallam University https://orcid.org/0000-0001-8156-5801

Mikołaj Ćwiok

University of Warsaw

Wojciech Dominik

University of Warsaw https://orcid.org/0000-0001-7444-9239

Aleksandra Fijałkowska

University of Warsaw

Mateusz Fila

University of Warsaw

Zenon Janas

University of Warsaw

Artur Kalinowski

University of Warsaw

Krzysztof Kierzkowski

University of Warsaw

Magdalena Kuich

University of Warsaw

Chiara Mazzocchi

Faculty of Physics, University of Warsaw https://orcid.org/0000-0003-2503-5413

Wojciech Okliński

University of Warsaw

Piotr Podlaski

University of Warsaw

Marcin Zaremba

University of Warsaw

Robin Smith

Sheffield Hallam University

Moshe Gai

University of Connecticut
Deran Schweitzer
University of Connecticut
Sean Finch
Duke University
Udo Friman-Gayer
Duke University
Samantha Johnson
University of North Carolina
Tyler Kowalewski
University of North Carolina
Dimiter Balabanski
RIKEN/ELI-NP, Horia Hulubei National Institute of Physics and Nuclear Engineering
https://orcid.org/0000-0003-2940-014X
Catalin Matei
Extreme Light Infrastructure - Nuclear Physics
Adrian Rotaru
Extreme Light Infrastructure - Nuclear Physics
Ross Allen
University of Birmingham
Mark Griffiths
University of Birmingham
Stuart Pirrie
University of Birmingham
Pedro Santa Rita Alcibia
University of Birmingham
Sarah Stern
University of Connecticut

Physical Sciences - Article

Keywords:

Posted Date: June 30th, 2026

DOI: https://doi.org/10.21203/rs.3.rs-10181237/v1

License: This work is licensed under a Creative Commons Attribution 4.0 International License.
Read Full License

Additional Declarations: There is **NO** Competing Interest.

Toward a Measurement of Stellar Oxygen Formation with the Warsaw Active Target TPC Operating in Gamma Beams

Kristian C. Z. Haverson*
School of Engineering and Built Environment, Sheffield Hallam University, Sheffield, S1 1WB, UK

Mikołaj Ćwiok,† Wojciech Dominik, Aleksandra Fijałkowska, Mateusz Fila, Zenon Janas, Artur Kalinowski, Krzysztof Kierzkowski, Magdalena Kuich, Chiara Mazzocchi, Wojciech Okliński, Piotr Podlaski, and Marcin Zaremba
Faculty of Physics, University of Warsaw, Warsaw, Poland

Robin Smith
School of Engineering and Built Environment, Sheffield Hallam University, Sheffield, S1 1WB, UK and
Laboratory for Nuclear Science at Avery Point, University of Connecticut, Groton, CT 06340, USA

Moshe Gai, Deran K. Schweitzer, and Sarah R. Stern
Laboratory for Nuclear Science at Avery Point, University of Connecticut, Groton, CT 06340, USA

Sean W. Finch and Udo Friman-Gayer
Department of Physics, Duke University, Durham, NC 27708, USA and
Triangle Universities Nuclear Laboratory, Durham, NC 27708, USA

Samantha R. Johnson‡ and Tyler M. Kowalewski
Department of Physics and Astronomy, University of North Carolina, Chapel Hill, NC 27599, USA and
Triangle Universities Nuclear Laboratory, Durham, NC 27708, USA

Dimiter L. Balabanski, Catalin Matei, and Adrian Rotaru
Extreme Light Infrastructure - Nuclear Physics (ELI-NP),
Horia Hulubei National Institute for R&D in Physics and Nuclear Engineering (IFIN-HH),
Reactorului Str.30, 077125 Bucharest-Magurele, Romania

Ross A. M. Allen, Mark R. Griffiths, Stuart Pirrie, and Pedro Santa Rita Alcibia
School of Physics and Astronomy, University of Birmingham, Edgbaston, B15 2TT, UK

(Dated: June 23, 2026)

Stellar formation of oxygen, the capture of alpha particles by ^{12}C, denoted as the $^{12}C(\alpha,\gamma)^{16}O$ reaction, is widely recognised as the most important nuclear input of stellar evolution theory. The cross section of this reaction at stellar energies, around 300 keV, determines the carbon-to-oxygen ratio (C/O) at the end of helium burning, a key parameter of this theory. Despite more than 50 years of measurements of angular distributions, current data, for the most part, fail to measure the interference of the $\ell = 1$ ($E1$) and the $\ell = 2$ ($E2$) partial waves, predicted by quantum mechanics. Previous measurements using the UConn–TUNL optical-readout TPC (O-TPC) in the HIγS gamma beam demonstrated the validity of measuring the direct $^{12}C(\alpha,\gamma_0)^{16}O$ reaction via the time-reversed photo-dissociation reaction, $^{16}O(\gamma,\alpha_0)^{12}C$. The current work presents a significantly improved measurement using the Warsaw electronic-readout TPC, which operates at much higher rates and with over 1,000 readout channels, enabling 4π three-dimensional reconstruction of nuclear events. Background-free angular distributions measured at centre-of-mass energies 1.46−2.72 MeV are reported, with $E1 - E2$ interference angles agreeing with quantum mechanical predictions over the entire measured energy range, motivating future measurements at lower energies to extrapolate the cross section to stellar conditions.

* K.Haverson@shu.ac.uk; khaverson@camk.edu.pl; These authors contributed equally to this work; Present address: Astrocent, Nicolaus Copernicus Astronomical Center of the Polish Academy of Sciences, Rektorska 4, 00-614 Warsaw, Poland
† mikolaj.cwiok@fuw.edu.pl; These authors contributed equally to this work.
‡ Present address: Department of Physics, North Carolina State University, Raleigh, North Carolina 27695-8202, USA and Triangle Universities Nuclear Laboratory, Duke University, Durham, North Carolina 27708, USA

I. INTRODUCTION

Stellar evolution theory has reached sufficient accuracy to allow the use of stars for measurements in fundamental physics. A notable example is the standard solar model (SSM) [1] that led to the discovery of neutrino oscillation [2]. Despite this progress, modelling supernova explosions remain a major challenge. The progenitors of both Type Ia (SNeIa) and Type II (SNII) supernovae still include a substantial unknown nuclear input: the carbon-to-oxygen ratio (C/O). This ratio is determined by the cross-section for the capture of an alpha-particle by ^{12}C to form ^{16}O, denoted as the ^{12}C$(\alpha,\gamma)^{16}$O reaction. This cross section was declared by Fowler to be of "paramount importance" for nuclear astrophysics [3], yet it remains ill-determined with insufficient accuracy, as discussed below. It is noteworthy that Hoyle had already emphasised the significance of the ^{12}C$(\alpha,\gamma)^{16}$O reaction in his seminal paper predicting the triple-alpha process [4], wherein he stated: "It can be shown that reaction [25, ^{12}C(α,γ)] is the most effective in destroying ^{12}C. Hence, to decide how far ^{12}C accumulates, it is necessary to compare the rates of reactions [24, $3\alpha \rightarrow {}^{12}$C] and [25, ^{12}C$(\alpha,\gamma)$]".

The C/O ratio determines the nickel core that drives the shape of the light curves of SNeIa [5]. Nevertheless, observations of SNeIa light curves are used to measure cosmological distances from which the accelerated expansion of the universe was discovered [6, 7]. This discovery relies on a yet to be understood empirical calibration [8] of the light curve to yield the absolute magnitude. The C/O ratio also determines whether SNII lead to a black hole (BH) or neutron star (NS) [9]. Of particular interest is whether SN1987A, a Type II SN explosion governed by neutrinos of the progenitor 20 $M_\odot$ Sanduleak blue giant star, ended up as a BH.

It was suggested [10] that a soft equation of state (EOS) of nuclear matter, that might arise from exotic nuclear matter such as Kaon condensate at the centre of the dense nuclear matter, would lead 1987A to a NS that will immediately collapse to a (rather light) stellar BH. Recent observations of blue light by the James Webb Space Telescope at the location of SN1987A [11], while not conclusive, suggest a NS at the location of SN1987A. If so, SN1987A could provide the lower mass limit of $\sim 20M_\odot$ for progenitor stars leading to a BH.

The C/O ratio of the progenitor star plays an equally important role as the EOS in determining whether a Type II SN ends up as a BH [9]. In sharp contrast to the repeated declaration of the importance of the ^{12}C(α,γ) reaction by Hoyle in 1954 [4], and then by Fowler in 1984, still today we observe inconsistencies in measurements of the gamma-ray emitted from the radiative capture of ^{12}C with an alpha particle– the ^{12}C(α,γ) reaction.

Ever since the seminal work of Dyer and Barnes [12] many measurements of the ^{12}C(α,γ) reaction were carried out [13–20]. In many previous publications, including previous TPC measurements of the time-reverse reaction [19, 20], a good agreement of the total reaction cross section is observed. However, the total reaction cross section alone cannot be used to extrapolate the cross section to stellar conditions, i.e. ∼300 keV. The $E1$ and $E2$ partial cross sections have different energy dependences and must be extrapolated separately. In particular, the $E1$ cross section at stellar energies is derived from an interference of the bound and quasi-bound 1^- states in ^{16}O at 7.117 and 9.585 MeV, respectively, but the $E2$ is mainly due to the bound 2^+ state at 6.917 MeV.

In contrast to the agreement observed for the total reaction cross section, measurements of the angular distributions, which are used to extract the $E1$ and $E2$ contributions, do not reveal a clear picture. Of concern is the $E1$–$E2$ mixing phase angle (ϕ_{12}) extracted from the partial wave decomposition of these angular distributions. It is either ill-determined (with an error bar close to 100%) or as shown by Gai [21], in disagreement with the elementary prediction of quantum mechanics [22, 23]

$$\phi_{12} = \delta_2 - \delta_1 + \tan^{-1}\frac{\eta}{2}, \tag{1}$$

where δ_1 and δ_2 are the p- and d- waves elastic scattering phase shifts, and η is the Sommerfeld parameter [24].

Ouellet *et al.* noted in their footnote b of Table II [14] that ϕ_{12} could "not [be] determined from the data", emphasising the need for more accurate data. Assunção, *et al.* [16] deduce $E1/E2$ ratios that are different by up to a factor of 5 when ϕ_{12} is considered a fit parameter or fixed as predicted from equation (1). Nevertheless, the best fit (three-parameter fit) results in all nine ϕ_{12} values measured below 2.2 MeV that disagree with predictions using equation (1). Notably, Plag *et al.* [18] measured ϕ_{12} values in agreement with equation (1). However, they did not measure data spanning the 1^- resonance (∼2.3 MeV) where one needs to demonstrate the additional sensitivity required to measure the rapidly varying ϕ_{12}, as pointed out by Ouellett *et al.* [14].

Measurements of gamma-rays emitted from the ^{12}C(α,γ) reaction suffer from a large neutron background due to the ^{13}C$(\alpha$,n) reaction. At 1.0 MeV, the (α,n) cross section is nine orders of magnitude larger than the (α,γ). Plag *et al.* [18] reduced this background by depleting the ^{13}C content of the target by a factor of 10^4 and additionally used pulsed beams and fast BaF gamma-ray detectors to measure Time-of-flight (TOF) and exclude neutron-induced events. The work of Plag *et al.* demonstrates the major challenge presented to measurements of the ^{12}C(α,γ) reaction and furthermore highlights the steps required for successful future measurements. Importantly, since this source of background is beam related, measurements in an underground laboratory still need to take steps to address this overwhelming background.

A recent global R-matrix fit to the "world data" [25] deduced the cross section at the Gamow window. The gamma-capture data included in this study, among other data, are in disagreement with predictions of ϕ_{12}, and are

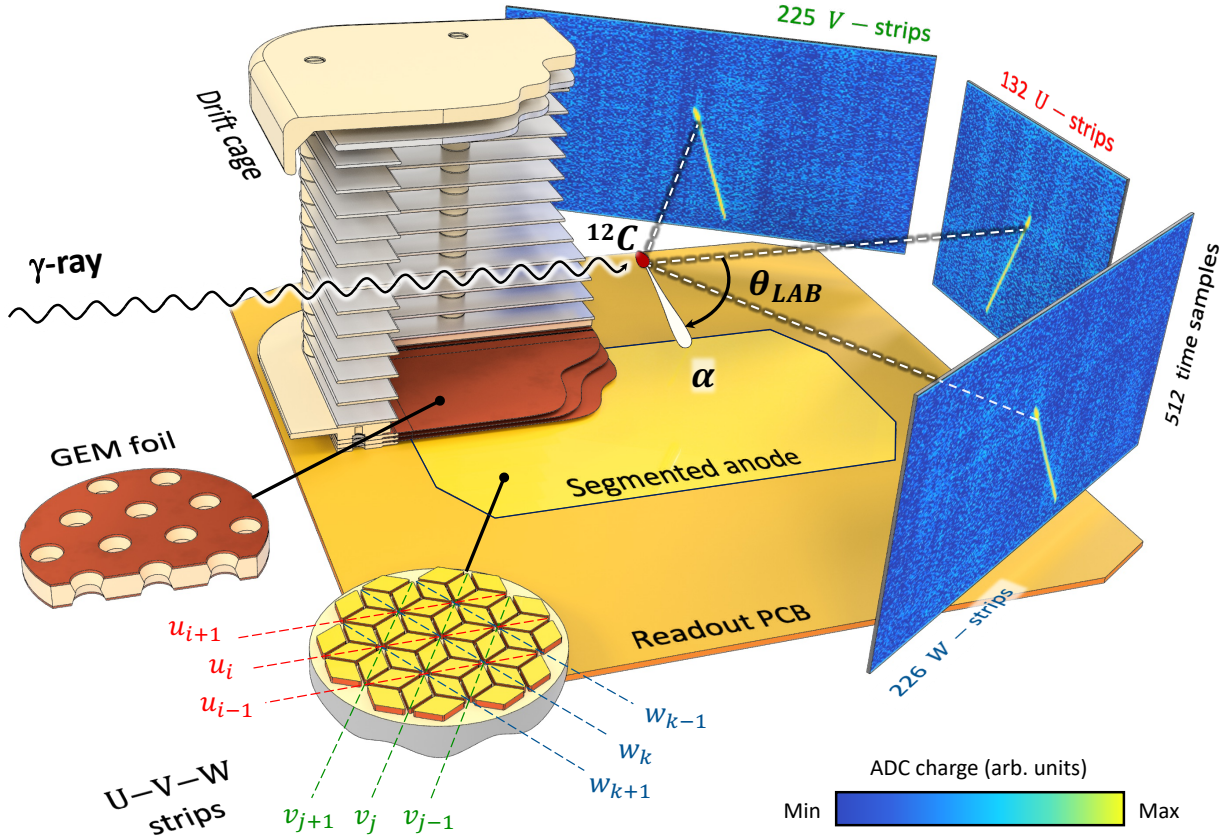


FIG. 1. **Visualisation of a ^{16}O photo-dissociation event measured by the Warsaw TPC.** A collimated quasi-monochromatic gamma beam enters the central part of the active TPC volume inside the gas vessel filled with pure CO_2 gas. One of the beam photons interacted with a ^{16}O nucleus of the gaseous target, yielding two charged particle tracks: α-particle (white) and ^{12}C ion (red). The resulting cloud of primary ionisation electrons drifts toward the anode in a uniform electric field created by a set of flat guarding electrodes that surround the fiducial volume. This primary charge is amplified by micro-pattern structures placed between the drift region and the segmented read-out anode. The inset in the bottom-left corner depicts details of diamond-shaped pads interconnected to form three rows of U, V and W anode strips crossed at 120°. Digitised signal waveforms collected by the front-end electronics are superimposed on the right-hand side as three histograms in *Strip*×*Time*×*Charge* domain. This information is combined to reconstruct the event's vertex position and momenta of the α-particle and the ion track. For clarity, only one quadrant of the actual TPC drift cage is shown in the upper-left corner of the figure.

inconclusive [21]. As such, the results are constrained by the Asymptotic Normalisation Coefficient (ANC), hence it is an Indirect Method. It is clear that precise measurements of the direct cross section of the ^{12}C(α,γ) reaction still remain.

To overcome these challenges we employ a new method where the time-reversed ^{16}O$(\gamma,\alpha)^{12}$C reaction is measured, from which the direct reaction ^{12}C$(\alpha,\gamma)^{16}$O is deduced using detailed balance [19, 20] (Methods A); Due to time reversal invariance, the shape of the angular distributions are identical to the gamma-ray distributions of the forward reaction. Therefore, this approach should not be regarded as an indirect method, nor a surrogate reaction. Furthermore, this approach allows us to measure only the ground state gamma decay (our method is insensitive to cascade gamma decay) and addresses the drawbacks of previous measurements as discussed above. The most significant being the removal of the large neutron-induced background.

We report measurements with the Warsaw active-target TPC detector operating in the gamma beams of the High Intensity γ-ray Source (HIγS). The TPC allows for measurements of complete angular distributions of the emitted charged particles over the entire $0° - 180°$ angular range, a feat not possible in typical gamma-ray experiments. We demonstrate that such measurements yield ϕ_{12} mixing angles that, for the first time, are consistent with the value predicted by quantum mechanics, equation (1), over the entire measured energy range of 1.46−2.72 MeV.

The present results, together with previous measurements using the UConn–TUNL O-TPC [19, 20], demonstrate the success of this method in determining the angular distributions of the ^{12}C$(\alpha,\gamma)^{16}$O reaction with unprecedented accuracy. The use of the Warsaw TPC detector in this work, however, demonstrates a significant

step forward in the methodology, overcoming the rate limitations of the O-TPC imposed by its optical read-out system and its inability to reconstruct true three-dimensional tracks. The advantages of the Warsaw TPC, demonstrated in previous reports [26–29] and confirmed in the present work, establish it as an ideal detector for extending measurements to lower energies, where data vital to extrapolating the cross section to stellar conditions can be obtained.

II. RESULTS

A. Gamma beam

A high-intensity ($\sim 4 \times 10^8$ γ/s), quasi-monochromatic gamma beam (FWHM$\sim$400 keV) was produced via Compton backscattering at the HIγS [30]. The beam intensities were the highest possible that could be provided by the facility. Fourteen nominal beam energies in the range $E_\gamma^{nom.} = 8.51$–13.9 MeV were used during the campaign, while results from seven in the range $E_\gamma^{nom.} = 8.51$–9.85 MeV are presented; these labels serve as run identifiers, with true energies listed in the Supplementary Material.

The beam intensity was continuously measured by means of a plastic scintillator counter positioned in the beam downstream of a 10.5-mm-diameter collimator, approximately 1.4 m upstream of the TPC detector. The efficiency of the plastic scintillator was determined in dedicated measurements; Further details are given in Methods B.

B. Warsaw time projection chamber

The Warsaw time projection chamber (TPC) [26–29] is a gaseous active-target time-projection chamber developed for studying photo-dissociation reactions at astrophysically-relevant energies, with the gas acting as both target and detection medium. It enables the full, unambiguous reconstruction of the momenta of the charged-particle products of the photo-dissociation reaction, thereby determining particle types, their energy and their emission angles. The latter are instrumental in disentangling the multipolarity of the transition. In brief, the gas medium is immersed in a uniform electric field, which causes the ionisation electrons generated by the charged particles along their trajectory to drift with constant velocity towards the anode. These electrons are then multiplied in the micro-pattern charge-amplification stages (Gas Electron Multipliers [31]) and collected at the segmented read-out anode of the detector by means of the fast front-end digitising electronics (General Electronics for TPCs [32, 33]). The U-V-W strip segmentation pattern together with the time distribution of the collected charge allows for tracing the charged particle trajectory and reconstructing its momentum. A schematic view of the TPC and its electronic read-out concept is shown in figure 1, while a detailed description can be found in Methods C. In the experiment, for the beam energies presented here, a high-purity CO_2 gas at an absolute pressure of 130 mbar was used.

C. Event topology & track reconstruction

Events recorded in the TPC were classified by track topology into three categories: 2- and 3-track events and minimal energy-deposit beam-induced events. The 2-track events correspond to the photo-dissociation of ^{16,17,18}O, and 3-track events to the photo-dissociation of ^{12}C. An example of raw data for a 2-track ^{16}O photo-dissociation event is displayed as inserts in figure 1.

In order to reconstruct the event, the main cluster of charge deposits was first identified in each U-V-W projection in the *Strip* $\times$ *Time* domain. Two examples of such cleaned events, for ^{16}O and ^{12}C photo-dissociation reactions, are shown as projections onto the W-strips in the upper and lower panels of figure 2, respectively. Background events that result in minimal energy being deposited in the detector (electronic noise, (γ, n)) were easily removed by setting a threshold on the integrated charge from the cleaned projections.

An algorithm was developed, as detailed in reference [34], to locate three key coordinates in each U-V-W projection. These are shown in figure 2, and are defined as: the event vertex p_{vertex} (brown point), the end of the α track p_α (orange point), and the so-called "ion end" p_{ion} (red point). For ^{12}C events, p_{ion} corresponds to the observed second-longest α track, which in some cases can represent two overlapping α tracks. For ^{16}O events, p_{ion} corresponds to the ^{12}C ion; the terms "ion length" and "ion end" refer to this shorter side of the track. Once these points in each projection were reconstructed independently, the data were paired based on the closest matching z-coordinate (common time axis across all projections) to obtain a three-dimensional Cartesian representation of the tracks.

Ion energy loss tables [35] were used to convert particle track lengths to energies. This enabled the full energy-momentum reconstruction of the long α track. Accounting for the momentum of the incident gamma beam, the nominal centre-of-mass energy and scattering angles of each event were obtained.

All track reconstruction procedures were validated using a detailed `Geant4` [36] Monte Carlo simulation reflecting the experimental conditions at each nominal beam energy. Simulated data were also used to derive event-by-event corrections for angle-dependent biases in the reconstructed scattering angles and to determine θ-dependent efficiency profiles, accounting for small reductions due to the data reduction cuts (discussed later). The angular distributions from the present analysis are further validated by the agreement with another independent analysis [37], measured using the full HIγS beam width.

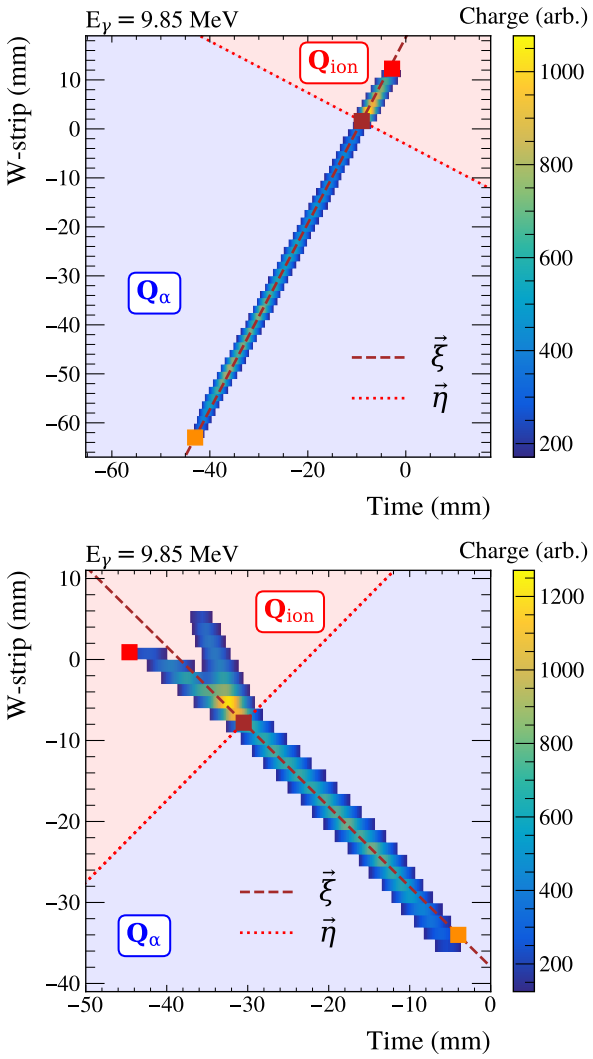


FIG. 2. **Event reconstruction.** Event projections onto W-strips after track isolation are shown for typical 2-track and 3-track events. **Top:** ^{16}O(γ,α_0) (2-track) event. **Bottom:** ^{12}C(γ,α_0) (3-track) event. Key positions are identified, these include the event vertex $p_{\rm vertex}$ (brown), α track end p_α (orange), and ion track end $p_{\rm ion}$ (red). The line $\hat{\xi}$ (brown dashed) is defined to pass through p_α and $p_{\rm vertex}$, and the line $\hat{\eta}$ (red dotted) is perpendicular to that passing though $p_{\rm vertex}$. This is used to define the separated charge regions of $Q_{\rm ion}$ (shaded red) and Q_α (shaded blue), which are used to calculate $Q_{\rm ratio}$.

D. Reaction channel separation

The majority of events, other than 2-track and 3-track topologies, were removed using integrated-charge cuts without reconstruction. The remaining photodissociation candidates (^{16}O, ^{17}O, ^{18}O, and ^{12}C) were then subjected to a sequence of software cuts to isolate a uniform sample of ^{16}O events. Fiducial volume cuts and their motivations are described in Methods D.

Key channel separation in the present work was achieved using several reconstructed quantities. An acceptance region in the ion-length vs alpha-length spectrum (figure 3a) cleanly rejected $^{17/18}$O(γ,α) background from the ^{16}O(γ,α) events, owing to the distinct Q-values of these reactions (6.359/6.228 MeV and 7.162 MeV respectively). Within this region, ^{16}O events populate the left feature and ^{12}C events the right. The remaining channels were separated using the $Q_{\rm ratio}$, which was determined by dividing the tracks along a line perpendicular to the $p_{\rm vertex}$–p_α axis, which passes through $p_{\rm vertex}$, as shown in figure 2. The charges in the α (shaded blue) and ion regions (shaded red) were used to define

$$Q_{\rm ratio} = \frac{Q_\alpha}{Q_\alpha + Q_{\rm ion}}. \qquad (2)$$

This metric provided excellent separation between key event types, capturing additional charge from the third non-reconstructed α-particle in the ^{12}C breakup without requiring explicit 3-track reconstruction. The $Q_{\rm ratio}$ as a function of $\cos\theta_{\rm lab}$ is shown in figure 3b, where the tilt of both features reflects the incident gamma beam momentum; the ^{16}O events were selected via the red shaded acceptance band.

A final cut was applied to the reconstructed centre-of-mass energies of the α ($E^\alpha_{\rm cm}$) and ion ($E^{\rm ion}_{\rm cm}$) tracks. Laboratory ion energies were converted to corresponding centre-of-mass energies under the assumption of ^{16}O(γ,α) kinematics. Events were required to fall within an elliptical region in the resulting two-dimensional $E^\alpha_{\rm cm}$ vs $E^{\rm ion}_{\rm cm}$ energy spectrum.

All selection criteria were either guided by a sample of data inspected visually [38] or detailed Monte Carlo simulations, where the latter was also used to quantify the ^{16}O reconstruction efficiency as a function of polar angle (typically ∼95%) and the residual ^{12}C contamination (typically 1 in 400 events); further details are provided in reference [34].

E. Cross sections

The TPC was calibrated using the known narrow states in ^{16}O at 9.845, 11.52, 12.44, and 13.09 MeV; this process is detailed in Methods E. The energy resolution of the TPC was determined using the narrow state at 9.85 MeV, yielding $\sigma \sim 55$ keV [34] for the automated analysis presented in this work, which was found to be consistent with $\sigma \sim 67$ keV [38] obtained in an independent manual analysis on a subset of events selected visually.

In the analysis of reference [38], data collected with the poor beam energy resolution (∼400 keV) were divided into considerably finer bins of 30 keV width. The centre-of-mass energy of each bin was reconstructed from the outgoing alpha particles detected in the TPC with

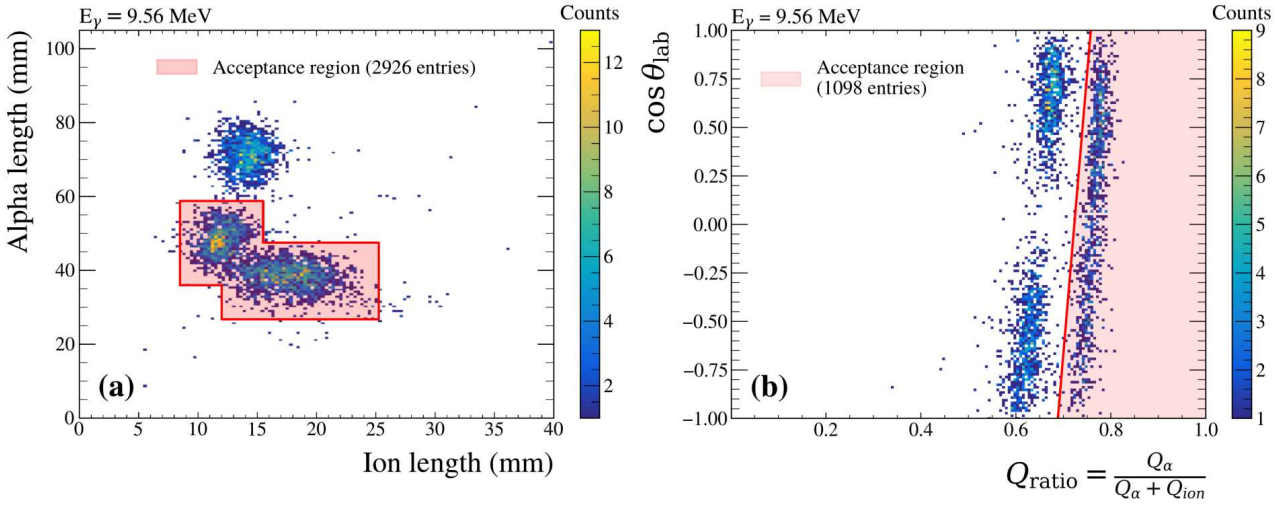


FIG. 3. **Reaction channel separation.** **(a)** Reconstructed alpha length versus ion length (opposite length) spectra showing separation of ^{16}O(γ,α) (left) and ^{12}C(γ,α) (right) events within the red acceptance region, with $^{17/18}$O(γ,α) events fully excluded (top). **(b)** $Q_{\rm ratio}$ versus $\cos\theta_{\rm lab}$ showing the $E2$-dominated ^{12}C(γ,α) events (left) and the $E1$–$E2$ mixing ^{16}O(γ,α) events (right). The red acceptance region gates on ^{16}O events.

the measured superior energy resolution. The so measured cross sections of the narrowly binned data exhibit variations by a factor of 100 over the energy range of $E_\gamma^{nom.} = 11.9$ MeV. This variation, which is predicted for the narrow (71 keV) 2^+ resonance at 11.52 MeV in ^{16}O, demonstrates our ability to measure large variations of the cross section over the broad beam energy width.

The following results pertain to the automated analysis of reference [34]. The remaining ^{16}O sample at each nominal beam energy were separately split into bins using the calibrated centre-of-mass energy. The ranges were chosen to ensure meaningful statistics when performing the partial wave decomposition. The centre-of-mass scattering angle, θ_{cm}, distributions for each bin were fitted using the partial-wave expansion for $E1$–$E2$ mixing, first shown by Dyer and Barnes [12]. This equation is shown here, re-parametrised as a ratio of cross sections

$$W(\theta) = W_{\rm E1}(\theta) + \frac{\sigma_{\rm E2}}{\sigma_{\rm E1}} W_{\rm E2}(\theta) + \sqrt{\frac{\sigma_{\rm E2}}{\sigma_{\rm E1}}}\cos(\phi_{12}) W_{12}(\theta), \quad (3)$$

where the terms are defined as

$$W_{\rm E1}(\theta) = P_0(\cos(\theta)) - P_2(\cos(\theta)),$$
$$W_{\rm E2}(\theta) = P_0(\cos(\theta)) + \frac{5}{7}P_2(\cos(\theta)) - \frac{12}{7}P_4(\cos(\theta)),$$
$$W_{12}(\theta) = \frac{6}{\sqrt{5}}\left(P_1(\cos(\theta)) - P_3(\cos(\theta))\right),$$

with P_ℓ being the Legendre polynomials.

Each angular distribution was fitted using unbinned negative log-likelihood minimisation with the `MINUIT` minimiser [39]. During fitting, Monte-Carlo-derived efficiency profiles were applied directly to the fit function to account for the data cuts and their effects on the angular distributions. These efficiency profiles are provided in the Supplementary Material. The level of ^{12}C contamination was sufficiently low to neglect background contributions. Asymmetric errors were obtained from likelihood contour plots. For visualisation, the data were binned, and the best fits were scaled accordingly, as shown in each panel of figure 4.

Even with the finer energy splitting of the data, the extracted parameters (angular distribution parameters and integrated cross sections) are still energy averaged; these are all listed in the Supplementary Material. For comparison with other datasets and theoretical fits, a deconvolution method was applied, as outlined in Methods F. The unfolded, angle-integrated cross sections were obtained by normalising the efficiency-corrected ^{16}O event counts in each angular distribution by the luminosity, as determined from the gold-foil analysis, distributed over the measured beam profile. The deconvolved values, goodness-of-fit score, and associated reconstructed effective energy and energy ranges are listed in table I.

The unfolded parameters are shown tracked in figure 5 as black data points with 1σ error bars. The results of the current analysis are compared with those from the literature. This enabled direct comparison with intrinsic theoretical predictions, shown as black dotted lines. Panel (a) shows the angle-integrated cross section and panel (b) shows the ratio of partial cross sections, both compared with the R-matrix prediction of reference [25]. Panel (c) shows the mixing phase angle ϕ_{12} compared with theoretical predictions using equation (1) based on the ^{12}C(α,α) elastic-scattering data of reference [40].

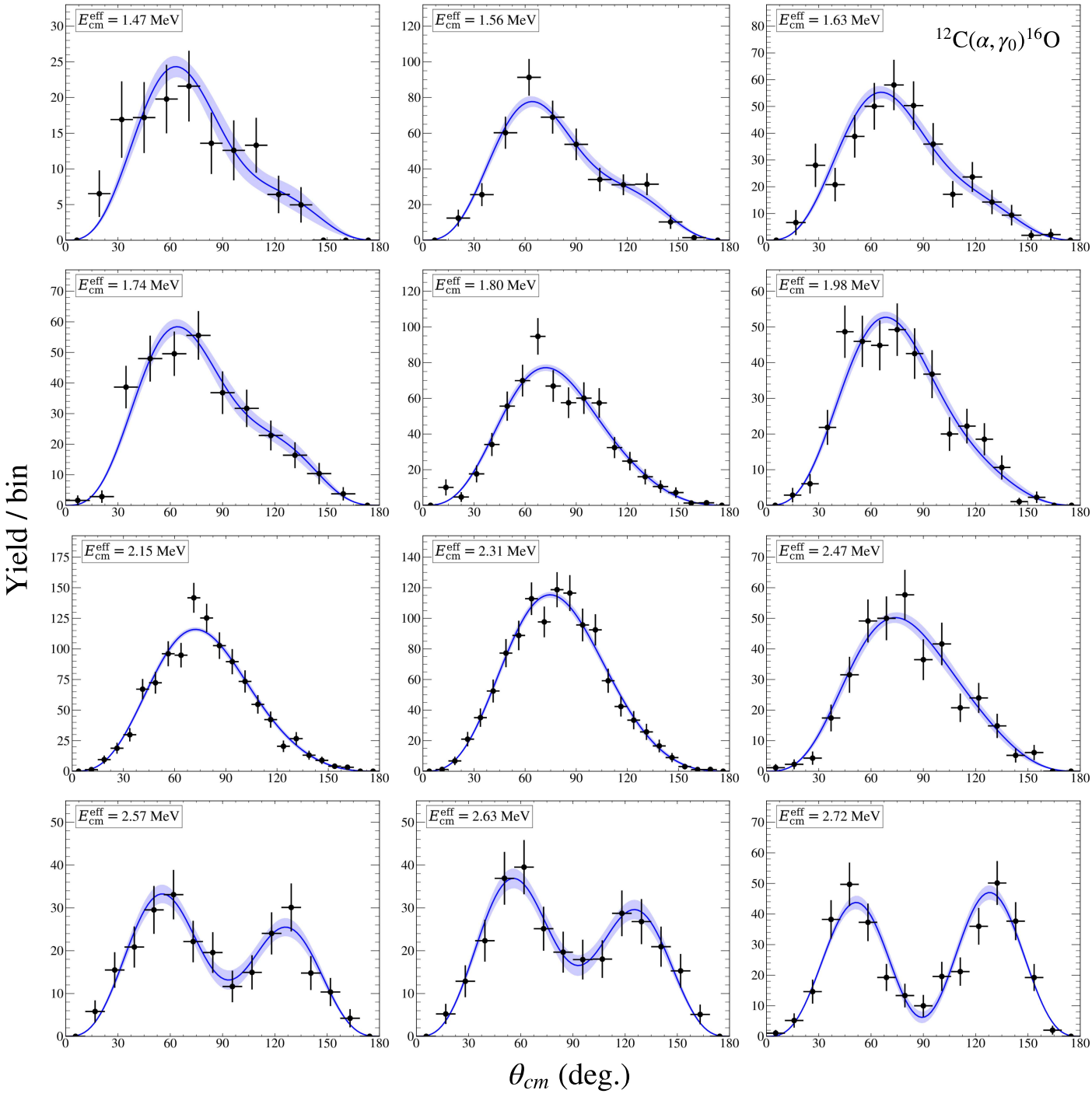


FIG. 4. **The ^{16}O$(\gamma,\alpha_0)^{12}$C angular distributions.** Each panel shows an angular distribution, ordered left to right, top to bottom, in terms of centre-of-mass energy. The black points represent the binned efficiency-corrected centre-of-mass scattering angle θ distributions measured by the Warsaw TPC. The blue line shows the fit of equation (3), with the shaded region indicating the 1σ uncertainty obtained from parameter covariances. The TPC-measured effective energy is given in each plot. The energy range considered for each distribution, the unfolded fit results, and goodness-of-fit statistics (χ^2_ν) are provided in table I.

$E_{\rm cm}^{\rm eff}$ (MeV)	$E_{\rm cm}$ range (MeV)	$E_\gamma^{nom.}$ (MeV)	$\frac{\sigma_{E2}}{\sigma_{E1}}$	ϕ_{12} (deg.)	$\sigma_{\alpha\gamma_0}$ (nb)	χ^2_ν
1.465(6)	1.25 , 1.65	8.51	$0.472\ ^{+0.268}_{-0.421}$	$56.0\ ^{+12.4}_{-10.9}$	0.51 (7)	0.86
1.559(3)	1.40 , 1.65	8.66	$0.439\ ^{+0.163}_{-0.209}$	$62.6\ ^{+5.9}_{-5.8}$	0.80 (9)	1.08
1.632(4)	1.40 , 1.70	8.86	$0.343\ ^{+0.164}_{-0.219}$	$57.8\ ^{+8.82}_{-7.8}$	1.4 (2)	1.10
1.739(4)	1.65 , 1.90	8.66	$0.425\ ^{+0.163}_{-0.216}$	$62.7\ ^{+6.6}_{-6.5}$	1.7 (2)	1.12
1.805(3)	1.70 , 1.90	8.86	$0.123\ ^{+0.073}_{-0.087}$	$49.3\ ^{+23.6}_{-9.2}$	2.5 (3)	1.02
1.979(3)	1.90 , 2.10	8.86	$0.197\ ^{+0.102}_{-0.130}$	$49.0\ ^{+14.8}_{-8.4}$	4.8 (6)	1.80
2.152(2)	2.00 , 2.30	9.16	$0.099\ ^{+0.045}_{-0.051}$	$37.2\ ^{+18.7}_{-7.8}$	16(2)	1.09
2.312(2)	2.15 , 2.50	9.36	$0.054\ ^{+0.030}_{-0.042}$	$12.2\ ^{+12.2}_{-4.2}$	42(5)	0.45
2.468(3)	2.40 , 2.55	9.56	$0.106\ ^{+0.077}_{-0.097}$	$57.3\ ^{+23.9}_{-8.8}$	37 (4)	1.15
2.575(4)	2.40 , 2.65	9.85	$0.295\ ^{+0.096}_{-0.146}$	$70.2\ ^{+6.0}_{-5.9}$	26 (3)	0.54
2.630(4)	2.55 , 2.70	9.56	$0.327\ ^{+0.099}_{-0.143}$	$77.1\ ^{+5.8}_{-5.8}$	20 (2)	0.39
2.719(3)	2.65 , 2.90	9.85	$0.059\ ^{+0.028}_{-0.051}$	$92.4\ ^{+8.0}_{-8.6}$	12 (1)	1.41

TABLE I. **Unfolded cross-section results.** The energy, $E_{\rm cm}^{\rm eff}$, corresponds to the average energy of all events in the energy slice considered (see Supplementary Material). All energy slices considered correspond to statistically independent event samples. The nominal beam energy, $E_\gamma^{nom.}$, is given as a run identifier. The partial-wave decomposition parameters ϕ_{12} and σ_{E2}/σ_{E1} are shown after application of the deconvolution method. The angle-integrated cross section σ_{α,γ_0} is shown after applying the detailed-balance factor and performing the deconvolution procedure. χ^2_ν is the goodness-of-fit statistic for the angular distribution.

III. DISCUSSION AND CONCLUSIONS

Extrapolation of the ^{12}C$(\alpha,\gamma_0)^{16}$O reaction cross section from laboratory energies, measurable in nuclear experiments, down to the astrophysically relevant Gamow energy window is crucial for predicting oxygen formation during helium burning, and has a tremendous knock-on effect across many stages of stellar evolution. However, these analyses present a significant challenge. Such extrapolations are achieved using R-matrix fits to the experimental data, and thus their validity hinges on the quality of measured partial cross sections at laboratory energies. Extrapolations of this cross section have hitherto relied on indirect methods of the cross sections, such as the ANC, which have poorly constrained uncertainties. The gold standard would centre such a fit on direct measurements of this cross section, which has not yet been possible.

To address these challenges, the current paper presents high-statistics precision angular distribution measurements of the ^{12}C$(\alpha,\gamma_0)^{16}$O reaction, obtained using gamma beams and the Warsaw TPC. In contrast with many of the data measured over the last 50 years using helium beams and gamma-ray detectors, the current measurements, along with earlier work using the O-TPC [19, 20], show unambiguous agreement of the extracted $E1$–$E2$ mixing phase angle ϕ_{12} with the values extracted from elastic scattering data. Such an agreement is crucial and demonstrates the absence of the systematic effects that biased some of the earlier data sets, which affect the shape of the angular distributions.

Although the main manuscript presents a summary of the experimental results, the data reported in the manuscript, together with the description of the experimental response, contain the information required for theoreticians to incorporate our measurements into a global R-matrix analysis. Unlike earlier data sets, we present unbinned energy-angle data that could be utilised in an unbinned R-matrix fit using a platform like `BRICK` [41], to permit more precise extrapolations of the cross section.

The demonstrated ability to measure the centre-of-mass energy of each event, as was presented in references [20, 38], represents a significant step forward, overcoming the long-standing limitations pertaining to the finite energy width of the gamma beam – an intractable issue at all gamma beam facilities. The TPC technique used in these experiments allows for background-free detection of rare reactions thanks to the unambiguous topological reconstruction of events. The successful measurements and excellent detection capabilities of the Warsaw TPC provide a strong motivation to use the same experimental setup to measure cross sections at centre-of-mass energies below 1.5 MeV. Further measurements of this reaction are planned at the HIγS with intensities several times higher than in the current work. Reaching cross sections at centre-of-mass energies well below 1 MeV will be possible with the next-generation laser Compton source delivering intensities of about $10^{11}\,\gamma$/s, which is being considered for a future upgrade of HIγS [42].

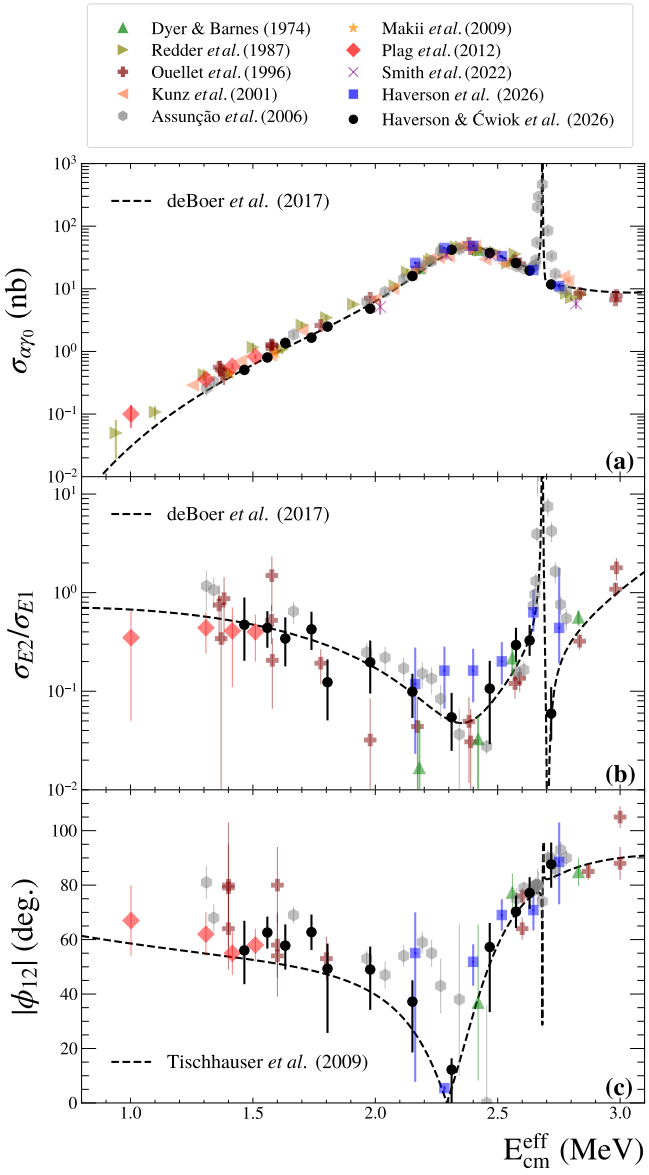


FIG. 5. **Summary of world data for the ^{12}C$(\alpha,\gamma)^{16}$O reaction.** **(a)** Integrated ground-state cross section compared with results from radiative-capture experiments and previous TPC studies, once unfolded. The dotted black line shows the current R-matrix fit to the world data from reference [25]. **(b)** Ratio of partial cross sections σ_{E2}/σ_{E1} compared with the theoretical prediction from reference [25] (black dotted line). **(c)** Partial-wave mixing angle ϕ_{12} obtained from angular-distribution fits in which ϕ_{12} was treated as a free parameter. The dotted black line shows the theoretical prediction obtained from equation (1) and the ^{12}C(α,α) elastic-scattering data of reference [40].

IV. METHODS

A. Detailed balance

The shape of the differential cross sections obtained from the radiative capture and photo-dissociation reactions is identical due to time-reversal invariance of both strong nuclear and electromagnetic interactions [43]. However, the angle-integrated cross sections differ, but are simply related through the principle of detailed balance, provided the measurement covers all azimuthal angles. This energy-dependent detailed balance factor, $f_{\rm db}$, is the ratio of the capture, $\sigma_{\alpha\gamma}$, and photo-dissociation, $\sigma_{\gamma\alpha}$, cross sections. Their relation is calculable as [44]

$$\sigma_{\alpha\gamma}(E_{\rm cm}) = \frac{2(2J_{16\rm O}+1)}{(2J_{12\rm C}+1)(2J_\gamma+1)}\frac{k_\gamma^2}{k^2}\,\sigma_{\gamma\alpha}(E_{\rm cm}), \qquad (4)$$

where J_n denotes the angular momentum quantum numbers of nucleus n, and k_γ and k are the photon and relative $^{12}\mathrm{C}+\alpha$ wave numbers, respectively

$$k_\gamma = \frac{E_\gamma}{\hbar c}, \qquad k = \frac{\sqrt{2\mu E_{\rm cm}}}{\hbar}, \qquad (5)$$

with μ being the reduced mass of the $^{12}\mathrm{C}+\alpha$ system and $E_\gamma \approx E_{\rm cm}+Q$, where $\hbar$ and c have their usual definitions. Substituting the appropriate angular momentum values and simplifying, the detailed balance factor reduces to

$$f_{\rm db}(E_{\rm cm}) = \frac{\sigma_{\gamma\alpha}(E_{\rm cm})}{\sigma_{\alpha\gamma}(E_{\rm cm})} = \frac{E_\gamma^2}{c^2\,\mu\,E_{\rm cm}}. \qquad (6)$$

B. Gamma beam

The gamma beam passed through a 10.5 mm diameter lead collimator positioned 53 m downstream of the production point before entering the Warsaw TPC. Beam alignment was established using a laser system and a Bismuth Germanate (BGO) gamma camera, and was subsequently confirmed through reconstructed interaction vertex positions distributed along the TPC length. The beam was predominantly circularly polarised, as verified by the measured azimuthal distributions of reaction products from the $^{12}\mathrm{C}(\gamma,\alpha_0)$ and $^{16}\mathrm{O}(\gamma,\alpha_0)$ reactions.

The energy profile of the gamma beam was measured by directing an attenuated beam onto a 120% high-purity germanium HPGe detector (HPGe). The produced spectra typically contained a full-energy absorption peak overwhelmed by escape peaks and Compton background. To extract the true energy distribution of the beam, an unfolding procedure was applied using `HORST` code [45]. This required two inputs: the energy-calibrated HPGe spectrum and a `Geant4`-simulated response matrix. The key parameters for the simulation included a beam spot of 12 mm diameter (in the HPGe plane) and the physical offset of the HPGe detector from the beam centre

(20 mm). The algorithm worked by estimating the initial parameters for the underlying beam distribution, then iteratively convolving trial distributions with the detector response and fitting the result to the measured raw spectra. The iteration with the lowest χ^2 yielded the final unfolded spectrum.

The unfolded spectra were then fitted with skewed Gaussian distributions defined as

$$H(E_\gamma \mid \zeta, \omega, \alpha) = \frac{1}{\omega\sqrt{2\pi}} \exp\Big[-\frac{1}{2}\Big(\frac{E_\gamma - \zeta}{\omega}\Big)^2\Big] \times \left[1 + \mathrm{erf}\Big(\frac{\alpha(E_\gamma - \zeta)}{\omega\sqrt{2}}\Big)\right], \quad (7)$$

where, ζ is the location parameter, ω is the scale parameter, and α is the shape parameter controlling the skewness. The mean μ and standard deviation σ of the skewed Gaussian can be obtained as $\mu = \zeta + \omega\,\delta\sqrt{\frac{2}{\pi}}$ and $\sigma = \omega\sqrt{1 - \frac{2\delta^2}{\pi}}$ respectively, where $\delta = \frac{\alpha}{\sqrt{1+\alpha^2}}$. All beam profiles are provided in the Supplementary Material.

The beam intensity was continuously monitored during the experiment by means of a 1 mm thick plastic scintillator positioned in the beam about 1.4 m upstream from the TPC detector. The absolute efficiency of the scintillator counter was determined with a set of calibration measurements. A highly attenuated beam was directed into a large volume NaI detector with a well-known absolute efficiency. By correcting for the attenuation in the copper absorber, the beam intensity at zero attenuation was extracted and used to determine the efficiency of the scintillator counter. The energy dependence of the efficiency of the scintillation counter was determined by fitting a linear function to the measured efficiencies. This energy dependence was supported by `Geant4` simulations of the scintillator counter's response.

This analysis was validated by a series of measurements using photo-activation of gold targets. For each beam energy, a gold foil with a thickness of 25 μm and an area covering the entire beam spot was positioned at the exit window of the TPC and irradiated for about 4 hours. The irradiated target was then removed and transported to a low-background lab in situ, where the decay of ^{196}Au produced in the ^{197}Au(γ, n) reaction was measured with an accurately calibrated HPGe detector. The average beam intensity during the irradiation of the gold target was then inferred from the intensity of ^{196}Au decay radiation. Additionally, for an exploratory run at the lowest energy point, a fission chamber with ^{238}U target was inserted in the beam and used to determine the intensity via the known photofission cross-section. Both methods yielded results in agreement with those obtained from the scintillator system.

C. Warsaw time projection chamber

The Warsaw time projection chamber comprises a vacuum vessel inside which the drift cage, amplification structure and read-out electrode are placed, while read-out electronics is located on the outside of the vessel [29].

The inner structure defines the active volume of 196 mm height and $330\times200\,\mathrm{mm}^2$ area with chamfered corners at 30° and includes an aluminium cathode plate, a drift cage that defines and shapes the uniform electric field by means of 12 hollow aluminium electrodes equally spaced, as well as the read-out anode, which is preceded by a charge-amplification structure. The latter consists of a stack of three 50 μm-thick Gas Electron Multiplier (GEM) foils [31] spaced at 3 mm, providing a total charge gain of $10^3 - 10^4$ [26]. The geometry of field-shaping electrodes interconnected by a chain of hight-voltage resistors assured homogeneity of the drift electric field better than 1% in the entire active volume. The collimated gamma beam enters and exits the TPC through 25 mm-diameter Kapton windows (50- and 125 μm-thick, respectively) and is aligned with the central axis of the inner TPC structure. The 14 mm gap between adjacent electrodes is larger than the diameter of the gamma beam spot in the TPC plane (∼11 mm).

The anode, kept at ground potential, is a multi-layer PCB board, segmented into a set of three independent rows of strips (denoted as U, V and W) crossed at 120°, with a 1.5 mm pitch (see figure 1). Virtual pixels can be created unambiguously on a 2D plane by this redundant 3-coordinate system. It should be noted that the topology of events that can stem from this type of experiment is relatively simple, with a maximum of three particles expected as a result of a single photo-disintegration. The total amount of channels being read out is 1018 (i.e. 264 for U, 376 for V and 378 for W strips).

The data acquisition (DAQ) system is based on the General Electronics for TPCs (GET) [32] complemented by custom-developed electronics. The signals from the electrode are processed by four 256-channel ASIC and ADC (AsAd) front-end cards each comprising 4 ASIC for GET (AGET) chips. The signal sampling frequency was set to 25 MHz, the dynamic range to 120 fC and the characteristic shaping time at 232 ns. The 64-channel AGET chips are equipped with a switched capacitor array (SCA) acting as a circular analogue memory buffer of 512 time cells per channel. Upon trigger, the acquisition is stopped after some programmed delay and the SCA content is digitised by a 12-bit ADC on the AsAd card and processed by a custom DAQ module designed at the Faculty of Physics UW (z-COBO), which uses System on Chip architecture combining the Field Programmable Gate Array and the Hard Processor System parts. A maximum trigger rate of 80 Hz can be achieved when all waveforms are recorded without any zero-suppression using a single 1 Gbit/s Ethernet link.

The TPC was operated in so-called self-trigger mode. The collective analogue signal from the last GEM in the

amplification stage is processed by the standard NIM electronics, where it is amplified, shaped and run through a discriminator to provide the gate trigger-signal for the z-COBO module, which time-stamps each recorded event 10 ns precision. The optimal discriminator threshold is adjusted for each TPC high-voltage working point to achieve fully-efficient triggering of the light ions (e.g. α-particles, carbon recoil), while allowing for some admixture of events induced by purely electromagnetic interactions of the gamma beam with detector medium.

The recorded waveforms were processed offline on a channel-by-channel basis. The common non-linear baseline was corrected using 4 dedicated Fixed Pattern Noise channels embedded in each AGET chip. The remaining constant pedestals were subtracted by calculating the average from the first 25 time cells containing an empty portion of the signal. These general preprocessing steps are outlined in [33].

The channels were then mapped to obtain three 2D histograms in *Strip* $\times$ *Time* domain, representing projections of the three-dimensional Cartesian spatial charge distribution of the event onto the readout plane as a function of time — one for each strip family, as explained in figure 1. The 3D reconstruction of the particle track is then completed by combining these 2D projections with the information on the drift velocity of the electrons in the gas under the given conditions. The latter is measured in the laboratory for the same operational conditions as during the experiment (gas density and TPC operation voltages) and verified with predictions of the `MAGBOLTZ` code [46]. During the experiment, the high voltage applied to the TPC structure was set as to maintain the tracks from ^{16}O photo-disintegration reaction fully contained in the TPC active volume and within the memory buffer of the read-out electronics. As a result, the optimal electron drift velocity ranged from 0.39 to 0.5 cm/μs depending on the nominal gamma beam energy of the run.

The natural-abundance CO_2 gas of grade 5.0 (99.999% purity) was supplied from a high-pressure cylinder to the low-pressure gas system that includes a mass-flow-controller, a set of two manual gas-dosing valves, a proportional-integral-derivative pressure controller, five pressure sensors and a dry diaphragm pump. Remote operation of the whole system was possible through a dedicated Detector Control System, which allowed to remotely control high-voltages and gas pressure, as well as recording all working conditions like: voltages, currents, temperatures, gas flow and pressure. Further details can be found in [29].

D. Fiducial cuts

When employing the reaction channel separation, described in section II D, fiducial cuts were placed to ensure full capture of the analysed tracks inside the TPC, and to remove angle-biasing effects.

To ensure full track containment, events were rejected if any track end-point lay within 5 mm of the active detector border. Additional containment cuts excluded events with reconstructed z-coordinates within the first 25 time bins of the electronics window or with total reconstructed time lengths exceeding half the drift-cage length, ensuring events do not reach the cathode/anode plane(s). Non–beam-related background was further suppressed by requiring the reconstructed vertex to lie along the main beam axis, in the same plane as the readout.

A fiducial volume was imposed to limit the effective gas target length. This was tuned run-by-run for ^{16}O to maintain uniform angular acceptance. A small angular fiducial cut removed poorly reconstructed events that spanned too few strips (i.e. were aligned mainly in time), otherwise leading to reduced energy resolution. To account for the slight reduction of ^{16}O events from all relevant cuts, a θ dependent efficiency correction was applied during cross section (integrated and differential) analysis.

E. Systematic Uncertainties

1. Event Energy

The sources of systematic uncertainty in the reconstructed event energy arise from the `SRIM` [35] stopping power tables used to convert measured track lengths to particle energies. The dominant contribution comes from track diffusion, which causes a systematic overestimation of the track length and hence the reconstructed laboratory energy. The effect of boosting event energies from the laboratory to the centre-of-mass frame using the nominal beam energy was investigated using simulated data and found to have a negligible impact.

An energy calibration was performed using known states in ^{16}O at $E_x = 9.845$, 11.52, 12.44, and 13.09 MeV, assuming a linear dependence between reconstructed and true energy. The fitted scale factor is consistent with unity at 1.000(2), while the offset provides the dominant correction of $-0.24(1)$ MeV. The calibration fit and residuals are provided in the supplementary material.

2. Angular Distributions

A small systematic angular reconstruction bias was identified by analysing Monte-Carlo simulated events. The bias follows a sinusoidal dependence on angle up to a maximum shift of 1°. This arises due to track vertex and endpoint reconstruction being less well defined for certain track orientations in the TPC. The shape of the bias was quantified at each beam energy and a correction was applied to the experimental angular distributions.

3. Cross Section

The energy-averaged cross section reconstruction is sensitive to the shapes of the beam energy distributions. The statistical uncertainties on the beam profiles was propagated through the HORST unfolding and fitting procedure. However, systematic uncertainty arising from the choice of HORST unfolding parameters was not evaluated and represents a potential source of unquantified error.

The dominant contributions to the luminosity uncertainty are the systematic uncertainties associated with the ^{197}Au activation (8%), fission chamber (10%), and NaI (7%) measurements used in the efficiency calibration of the scintillator counter. The overall systematic uncertainty of the absolute beam intensity determination was estimated to be 9%. The systematic uncertainty on the target-thickness stability amounted to about 1%.

F. Energy averaging and the TPC Response

To compare the energy-averaged cross sections obtained in this work, an unfolding procedure is required. The general procedure is outlined in reference [47], which has been modified to suit the unique treatment of these TPC data. This should be kept in mind when these data are included in a global evaluation.

In the following sections, superscripts of † denote theoretical expectation values, $X(E)$ explicitly denotes energy-dependent values, $\langle X\rangle$ denotes energy-averaged quantities, and all energies are in the centre-of-mass frame.

a. TPC-reconstructed Effective Energy. For finely binned TPC data, an effective centre-of-mass energy, $E_{\rm eff}$, is defined for each energy slice, $[a,b]$, by averaging over events in this energy range. The following quantity, $E^{\dagger}_{\rm eff}$, represents the expectation value of this quantity

$$E^{\dagger}_{\rm eff} = \frac{\int_a^b E\left[\int_0^\infty H(E')\,\sigma^{\dagger}_{\gamma\alpha}(E')\,\mathcal{G}(E-E')\,dE'\right]dE}{\int_a^b\left[\int_0^\infty H(E')\,\sigma^{\dagger}_{\gamma\alpha}(E')\,\mathcal{G}(E-E')\,dE'\right]dE}, \tag{8}$$

where, $\mathcal{G}(E-E')$ represents the Gaussian TPC resolution, $H(E)$ is the parameterised beam profile, and $\sigma^{\dagger}_{\gamma\alpha}$ is a model of the photo-dissociation cross section.

b. Integrated Cross Section. The angle-integrated photo-dissociation cross section is typically obtained across the whole width of the beam, experimentally as

$$\sigma_{\gamma\alpha} = \frac{N}{\mathcal{L}}, \qquad \mathcal{L} = N_\gamma\, n\, x, \tag{9}$$

where N is the number of observed events, N_γ the number of incident photons, n the target number density, and x the target thickness.

For a finer binned measurement, the luminosity $\mathcal{L}$ can be distributed across the measured beam profile $H(E)$, and the efficiency-corrected TPC measurement $S(E)$ can be normalised accordingly. The expectation value of the TPC measurement, accounting for the detector resolution, is

$$S^{\dagger}(E) = \int \mathcal{L}\,H(E')\,\sigma^{\dagger}_{\gamma\alpha}(E')\,\mathcal{G}(E-E')\,dE'. \tag{10}$$

For a finite energy bin $[a,b]$, the experimental reconstructed effective cross section is

$$\langle\sigma_{\gamma\alpha}\rangle = \frac{\int_a^b S(E)\,dE}{\int_a^b\left[\int \mathcal{L}\,H(E')\,\mathcal{G}(E-E')\,dE'\right]dE}, \tag{11}$$

with the corresponding theoretical expectation value

$$\langle\sigma^{\dagger}_{\gamma\alpha}\rangle = \frac{\int_a^b\left[\int \mathcal{L}\,H(E')\,\sigma^{\dagger}_{\gamma\alpha}(E')\,\mathcal{G}(E-E')\,dE'\right]dE}{\int_a^b\left[\int \mathcal{L}\,H(E')\,\mathcal{G}(E-E')\,dE'\right]dE}. \tag{12}$$

It is noted, from the above equation, that the experimentally reconstructed cross section does not reduce to a simple Gaussian convolution of the underlying cross section. This is due to the resolution of the TPC measurement.

The correction factor relating the TPC-reconstructed cross section to the true cross section at the reconstructed effective energy is

$$f_{\rm cor} = \frac{\sigma^{\dagger}_{\gamma\alpha}(E_{\rm eff})}{\langle\sigma^{\dagger}_{\gamma\alpha}\rangle}. \tag{13}$$

The detailed balance factor, $f_{\rm db}$, is used as follows, to obtain the experimentally unfolded radiative capture cross section

$$\sigma_{\alpha\gamma} = \frac{\langle\sigma_{\gamma\alpha}\rangle f_{\rm cor}}{f_{\rm db}(E_{\rm eff})}. \tag{14}$$

c. Partial-wave decomposition. This section describes the corrections needed for the extracted angular distribution parameters. Let $\sigma_\lambda(E)$ denote the underlying partial cross section for angular momentum λ.

For a slice integrated over the whole beam profile, the expectation value is

$$\langle\sigma^{\dagger}_{\lambda}\rangle = \frac{\int_0^\infty \sigma^{\dagger}_{\lambda}(E)\,H(E)\,dE}{\int_0^\infty H(E)\,dE}. \tag{15}$$

Similarly, the expectation value of the interference term $\cos\phi_{12}$ between $E1$ and $E2$ contributions is

$$\langle\cos\phi^{\dagger}_{12}\rangle = \frac{\int_0^\infty \cos\phi^{\dagger}_{12}(E)\,\sqrt{\sigma^{\dagger}_1(E)\,\sigma^{\dagger}_2(E)}\,H(E)\,dE}{\sqrt{\langle\sigma^{\dagger}_1\rangle\,\langle\sigma^{\dagger}_2\rangle}\int_0^\infty H(E)\,dE}. \tag{16}$$

Accounting for finite TPC resolution and bin width $[a, b]$, the reconstructed partial cross sections become

$$\langle \sigma_\lambda^\dagger \rangle = \frac{\int_a^b \left[\int \sigma_\lambda^\dagger(E')\, H(E')\, \mathcal{G}(E - E')\, dE' \right] dE}{\int_a^b \left[\int H(E')\, \mathcal{G}(E - E')\, dE' \right] dE}, \quad (17)$$

and

$$\langle \cos \phi_{12}^\dagger \rangle \quad (18)$$

$$= \frac{\int_a^b \left[\int \cos \phi_{12}^\dagger(E') \sqrt{\sigma_1^\dagger(E')\, \sigma_2^\dagger(E')}\, H(E')\, \mathcal{G}(E - E')\, dE' \right] dE}{\sqrt{\langle \sigma_1^\dagger \rangle \langle \sigma_2^\dagger \rangle} \int_a^b \left[\int H(E')\, \mathcal{G}(E - E')\, dE' \right] dE}. \quad (19)$$

Thus, similarly to what was described previously, correction factors to unfold the TPC-reconstructed quantities can be obtained.

RIGHTS RETENTION STATEMENT

For the purpose of open access, the author has applied a Creative Commons Attribution (CC BY) license to any Author Accepted Manuscript version of this paper arising from this submission.

DATA AVAILABILITY

A set of files containing high-level reconstructed quantities is available in https://doi.org/****/shu-****. Low-level TPC data can be made available upon reasonable request.

CODE AVAILABILITY

Example analysis codes, written in ROOT C++, are available in this data repository: https://doi.org/****/shu-****.

ACKNOWLEDGMENTS

The authors thank the staff of HIγS at Triangle Universities Nuclear Laboratory for the providing high intensity stable beams through the whole beamtime. This research was funded by the US Department of Energy [grant numbers DE-FG02-94ER40870, DE-SC0005367, DE-FG02-97ER41033, DE-FG02-91ER-40608, and DE-FG02-97ER41041]; the Science and Technology Facilities Council [grant numbers ST/Y000331/1 and ST/V001086/1]; the National Science Centre, Poland (contract no. UMO-2019/33/B/ST2/02176) and by the Excellence Initiative – Research University of the University of Warsaw. Partial financial support was provided by the Romanian Ministry of Research, Innovation and Digitalization under contract no. PN 23 21 01 06 and the ELI-RO program, contract no. ELI-RO_RDI_2024_007 (ELITE). The Warsaw team would like to thank engineers R. Dąbrowski, H. Czyrkowski and P. Zbińkowski for their excellent technical support in constructing the Warsaw TPC detector.

AUTHOR CONTRIBUTIONS

K.C.Z. Haverson and M. Ćwiok contributed equally to this work as co-first authors. Data analysis and interpretation: KCZH, MG, RS, MC, WD, MF, ZJ, ChM. TPC system design and development: MC, WD. Data acquisition development and control software: MZ, MC, WO, KK, MK, MF. Development of data analysis methodology: KCZH, AK, MC, RS, MG. Monte Carlo code development and simulations: PP, MC, KCZH. Visual inspection of the data for algorithm validation: MC, WD, MK, ZJ, ChM, MF, DKS, SRS, MG, KCZH. Experiment installation and TPC system operation during the runs: MC, WD, MF, ZJ, MK, ChM, MG, KCZH. Participation in the data-taking: MC, KCZH, WD, AF, MF, ZJ, MK, ChM, MG, DKS, SRS, DLB, CM, AR, RAMA, MRG, SP, PSRA. Writing the initial draft: KCZH, MG. Support and assistance with experiment operations: SWF, UFG, SRJ, TMK. Spokespersons of the experiments: MG, WD. PhD advisors of KCZH: RS, MG.

COMPETING INTERESTS

The authors declare no competing interests.

MATERIALS & CORRESPONDENCE

The corresponding author to whom requests should be made is K. C. Z. Haverson.

[1] J. N. Bahcall, *Neutrino Astrophysics* (Cambridge University Press, 1989).
[2] A. B. McDonald, Review of Modern Physics **88**, 030502 (2016).
[3] W. A. Fowler, Review of Modern Physics **56**, 149 (1984).
[4] F. Hoyle, Astrophysical Journal Supplement **1**, 121 (1954).
[5] F.-K. Thielemann, F. Brachwitz, P. Höflich, G. Martinez-Pinedo, and K. Nomoto, New Astronomy Reviews **48**, 605 (2004).

[6] A. G. Riess, A. V. Filippenko, P. Challis, A. Clocchiatti, A. Diercks, P. M. Garnavich, R. L. Gilliland, C. J. Hogan, S. Jha, R. P. Kirshner, B. Leibundgut, M. M. Phillips, D. Reiss, B. P. Schmidt, R. A. Schommer, R. C. Smith, J. Spyromilio, C. Stubbs, N. B. Suntzeff, and J. Tonry, Astronomical Journal **116**, 1009 (1998).

[7] S. Perlmutter, G. Aldering, G. Goldhaber, R. A. Knop, P. Nugent, P. G. Castro, S. Deustua, S. Fabbro, A. Goobar, D. E. Groom, I. M. Hook, A. G. Kim, M. Y. Kim, J. C. Lee, N. J. Nunes, R. Pain, C. R. Pennypacker, R. Quimby, C. Lidman, R. S. Ellis, M. Irwin, R. G. McMahon, P. Ruiz-Lapuente, N. Walton, B. Schaefer, B. J. Boyle, A. V. Filippenko, T. Matheson, A. S. Fruchter, N. Panagia, H. J. M. Newberg, W. J. Couch, and T. S. C. Project, Astrophysical Journal **517**, 565 (1999).

[8] M. M. Phillips, Astrophysical Journal Letters **413**, L105 (1993).

[9] T. A. Weaver and S. E. Woosley, Physics Reports **227**, 65 (1993).

[10] G. E. Brown, S. W. Bruenn, and J. C. Wheeler, Comments on Astrophysics **16**, 153 (1992).

[11] C. Fransson, M. J. Barlow, P. J. Kavanagh, J. Larsson, O. C. Jones, B. Sargent, M. Meixner, P. Bouchet, T. Temim, G. S. Wright, J. A. D. L. Blommaert, N. Habel, A. S. Hirschauer, J. Hjorth, L. Lenkić, T. Tikkanen, R. Wesson, A. Coulais, O. D. Fox, R. Gastaud, A. Glasse, J. Jaspers, O. Krause, R. M. Lau, O. Nayak, A. Rest, L. Colina, E. F. van Dishoeck, M. Güdel, T. Henning, P.-O. Lagage, G. Östlin, T. P. Ray, and B. Vandenbussche, Science **383**, 898 (2024).

[12] P. Dyer and C. A. Barnes, Nuclear Physics A **233**, 495 (1974).

[13] A. Redder, H. W. Becker, C. Rolfs, H. P. Trautvetter, T. R. Donoghue, T. C. Rinckel, J. W. Hammer, and K. Langanke, Nuclear Physics A **462**, 385 (1987).

[14] J. M. L. Ouellet, M. N. Butler, H. C. Evans, H. W. Lee, J. R. Leslie, J. D. MacArthur, W. McLatchie, H.-B. Mak, P. Skensved, J. L. Whitton, X. Zhao, and T. K. Alexander, Physical Review C **54**, 1982 (1996).

[15] R. Kunz, M. Jaeger, A. Mayer, J. W. Hammer, G. Staudt, S. Harissopulos, and T. Paradellis, Physical Review Letters **86**, 3244 (2001).

[16] M. Assunção, M. Fey, A. Lefebvre-Schuhl, J. Kiener, V. Tatischeff, J. W. Hammer, C. Beck, C. Boukari-Pelissie, A. Coc, J. J. Correia, S. Courtin, F. Fleurot, E. Galanopoulos, C. Grama, F. Haas, F. Hammache, F. Hannachi, S. Harissopulos, A. Korichi, R. Kunz, D. LeDu, A. Lopez-Martens, D. Malcherek, R. Meunier, T. Paradellis, M. Rousseau, N. Rowley, G. Staudt, S. Szilner, J. P. Thibaud, and J. L. Weil, Physical Review C **73**, 055801 (2006).

[17] H. Makii, Y. Nagai, T. Shima, M. Segawa, K. Mishima, H. Ueda, M. Igashira, and T. Ohsaki, Physical Review C **80**, 065802 (2009).

[18] R. Plag, R. Reifarth, M. Heil, F. Käppeler, G. Rupp, F. Voss, and K. Wisshak, Physical Review C **86**, 015805 (2012).

[19] R. Smith, M. Gai, S. R. Stern, D. K. Schweitzer, and M. W. Ahmed, Nature Communications **12**, 5920 (2021).

[20] K. C. Haverson, R. Smith, M. Gai, D. K. Schweitzer, S. R. Stern, and S. W. Finch, Communications Physics **9**, 27 (2026).

[21] M. Gai, Current Data on the $^{12}C(\alpha,\gamma)$ Reaction; a Critical Review and the Road Map Ahead, XLVII Symposium on Nuclear Physics, Cocoyoc, Morelos, Mexico, January 6–9, (2026), EPJ Web of Conferences, to Be Published.

[22] C. R. Brune, Physical Review C **64**, 055803 (2001).

[23] M. Gai, Physical Review C **88**, 062801 (2013).

[24] J. M. Blatt and V. F. Weisskopf, *Theoretical nuclear physics* (Springer, New York, 1952).

[25] R. J. de Boer, J. Görres, M. Wiescher, R. E. Azuma, A. Best, C. R. Brune, C. E. Fields, S. Jones, M. Pignatari, D. Sayre, K. Smith, F. X. Timmes, and E. Uberseder, Review of Modern Physics **89**, 035007 (2017).

[26] M. Ćwiok, M. Bieda, J. S. Bihałowicz, W. Dominik, Z. Janas, Ł. Janiak, J. Mańczak, T. Matulewicz, C. Mazzocchi, M. Pfützner, P. Podlaski, S. Sharma, M. Zaremba, D. Balabanski, A. Bey, D. G. Ghita, O. Tesileanu, and M. Gai, Acta Physica Polonica B **49**, 509 (2018).

[27] M. Gai, D. Schweitzer, S. R. Stern, A. H. Young, R. Smith, M. Cwiok, J. S. Bihalowicz, H. Czyrkowski, R. Dabrowski, W. Dominik, A. Fijalkowska, Z. Janas, L. Janiak, A. Korgul, T. Matulewicz, C. Mazzocchi, M. Pfuetzner, M. Zaremba, D. Balabanski, I. Gheorghe, C. Matei, O. Tesileanu, N. V. Zamfir, M. W. Ahmed, S. S. Henshaw, C. R. Howell, J. M. Mueller, L. S. Myers, S. Stave, C. Sun, H. R. Weller, Y. K. Wu, A. Breskin, V. Dangendorf, K. Tittelmeier, and M. Freer, Nucl. Inst. Meth A **954**, 161779 (2020).

[28] M. Ćwiok, W. Dominik, A. Fijałkowska, M. Fila, Z. Janas, A. Kalinowski, K. Kierzkowski, M. Kuich, C. Mazzocchi, W. Okliński, M. Zaremba, M. Gai, D. K. Schweitzer, S. R. Stern, S. Finch, U. Friman-Gayer, S. R. Johnson, T. M. Kowalewski, D. L. Balabanski, C. Matei, A. Rotaru, K. C. Haverson, R. Smith, R. A. Allen, M. R. Griffiths, S. Pirrie, and P. Santa Rita Alcibia, EPJ Web of Conferences **279**, 04002 (2023).

[29] M. Ćwiok, W. Dominik, A. Fijałkowska, M. Fila, Z. Janas, A. Kalinowski, K. Kierzkowski, M. Kuich, C. Mazzocchi, W. Okliński, P. Podlaski, M. Zaremba, M. Gai, S. R. Stern, D. K. Schweitzer, and D. L. Balabanski, EPJ Web of Conferences **290**, 01004 (2023).

[30] H. R. Weller, M. W. Ahmed, H. Gao, W. Tornow, Y. K. Wu, M. Gai, and R. Miskimen, Progress in Particle and Nuclear Physics **62**, 257 (2009).

[31] F. Sauli, Nucl. Inst. Meth A **386**, 531 (1997).

[32] E. C. Pollacco, G. F. Grinyer, F. Abu-Nimeh, T. Ahn, S. Anvar, A. Arokiaraj, Y. Ayyad, H. Baba, M. Babo, P. Baron, D. Bazin, S. Beceiro-Novo, C. Belkhiria, M. Blaizot, B. Blank, J. Bradt, G. Cardella, L. Carpenter, S. Ceruti, E. De Filippo, E. Delagnes, S. De Luca, H. De Witte, F. Druillole, B. Duclos, F. Favela, A. Fritsch, J. Giovinazzo, C. Gueye, T. Isobe, P. Hellmuth, C. Huss, B. Lachacinski, A. T. Laffoley, G. Lebertre, L. Legeard, W. G. Lynch, T. Marchi, L. Martina, C. Maugeais, W. Mittig, L. Nalpas, E. V. Pagano, J. Pancin, O. Poleshchuk, J. L. Pedroza, J. Pibernat, S. Primault, R. Raabe, B. Raine, A. Rebii, M. Renaud, T. Roger, P. Roussel-Chomaz, P. Russotto, G. Saccà, F. Saillant, P. Sizun, D. Suzuki, J. A. Swartz, A. Tizon, A. Trifiró, N. Usher, G. Wittwer, and J. C. Yang, Nucl. Inst. Meth A **887**, 81 (2018).

[33] J. Giovinazzo, T. Goigoux, S. Anvar, P. Baron, B. Blank, E. Delagnes, G. F. Grinyer, J. Pancin, J. L. Pedroza,

J. Pibernat, E. Pollacco, A. Rebii, T. Roger, and P. Sizun, Nucl. Inst. Meth A **840**, 15 (2016).

[34] K. C. Z. Haverson, Photo-dissociation for studying the astrophysical $^{12}C(\alpha,\gamma)^{16}O$ reaction and the structure of ^{12}C, sheffield Hallam University, Doctoral Thesis (2025).

[35] J. F. Ziegler, M. D. Ziegler, and J. P. Biersack, Nucl. Inst. Meth B **268**, 1818 (2010).

[36] S. Agostinelli, J. Allison, K. Amako, J. Apostolakis, H. Araujo, P. Arce, M. Asai, D. Axen, S. Banerjee, G. Barrand, F. Behner, L. Bellagamba, J. Boudreau, L. Broglia, A. Brunengo, H. Burkhardt, S. Chauvie, J. Chuma, R. Chytracek, G. Cooperman, G. Cosmo, P. Degtyarenko, A. Dell'Acqua, G. Depaola, D. Dietrich, R. Enami, A. Feliciello, C. Ferguson, H. Fesefeldt, G. Folger, F. Foppiano, A. Forti, S. Garelli, S. Giani, R. Giannitrapani, D. Gibin, J. J. Gómez Cadenas, I. González, G. Gracia Abril, G. Greeniaus, W. Greiner, V. Grichine, A. Grossheim, S. Guatelli, P. Gumplinger, R. Hamatsu, K. Hashimoto, H. Hasui, A. Heikkinen, A. Howard, V. Ivanchenko, A. Johnson, F. W. Jones, J. Kallenbach, N. Kanaya, M. Kawabata, Y. Kawabata, M. Kawaguti, S. Kelner, P. Kent, A. Kimura, T. Kodama, R. Kokoulin, M. Kossov, H. Kurashige, E. Lamanna, T. Lampén, V. Lara, V. Lefebure, F. Lei, M. Liendl, W. Lockman, F. Longo, S. Magni, M. Maire, E. Medernach, K. Minamimoto, P. Mora de Freitas, Y. Morita, K. Murakami, M. Nagamatu, R. Nartallo, P. Nieminen, T. Nishimura, K. Ohtsubo, M. Okamura, S. O'Neale, Y. Oohata, K. Paech, J. Perl, A. Pfeiffer, M. G. Pia, F. Ranjard, A. Rybin, S. Sadilov, E. Di Salvo, G. Santin, T. Sasaki, N. Savvas, Y. Sawada, S. Scherer, S. Sei, V. Sirotenko, D. Smith, N. Starkov, H. Stoecker, J. Sulkimo, M. Takahata, S. Tanaka, E. Tcherniaev, E. Safai Tehrani, M. Tropeano, P. Truscott, H. Uno, L. Urban, P. Urban, M. Verderi, A. Walkden, W. Wander, H. Weber, J. P. Wellisch, T. Wenaus, D. C. Williams, D. Wright, T. Yamada, H. Yoshida, and D. Zschiesche, Nucl. Inst. Meth A **506**, 250 (2003).

[37] S. Stern, TPC Operating in Gamma-beams: a New Tool for Nuclear Astrophysics, university of Connecticut, Doctoral Thesis (2026).

[38] M. Fila, Study of $^{16}O(\gamma,\alpha)^{12}C$ nuclear reaction with the Warsaw TPC detector, university of Warsaw, Doctoral Thesis (2024).

[39] F. James and M. Roos, Computer Physics Communications **10**, 343 (1975).

[40] P. Tischhauser, A. Couture, R. Detwiler, J. Görres, C. Ugalde, E. Stech, M. Wiescher, M. Heil, F. Käppeler, R. E. Azuma, and L. Buchmann, Physical Review C **79**, 055803 (2009).

[41] D. Odell, C. R. Brune, D. R. Phillips, R. J. de Boer, and S. N. Paneru, Frontiers in Physics **10**, 888476 (2022).

[42] C. R. Howell, M. W. Ahmed, A. Afanasev, D. Alesini, J. R. M. Annand, A. Aprahamian, D. L. Balabanski, S. V. Benson, A. Bernstein, C. R. Brune, J. Byrd, B. E. Carlsten, A. E. Champagne, S. Chattopadhyay, D. Davis, E. J. Downie, J. M. Durham, G. Feldman, H. Gao, C. G. R. Geddes, H. W. Grießhammer, R. Hajima, H. Hao, D. Hornidge, J. Isaak, R. V. F. Janssens, D. P. Kendellen, M. A. Kovash, P. P. Martel, U.-G. Meißner, R. Miskimen, B. Pasquini, D. R. Phillips, N. Pietralla, D. Savran, M. R. Schindler, M. H. Sikora, W. M. Snow, R. P. Springer, C. Sun, C. Tang, B. Tiburzi, A. P. Tonchev, W. Tornow, C. A. Ur, D. Wang, H. R. Weller, V. Werner, Y. K. Wu, J. Yan, Z. Zhao, A. Zilges, and F. Zomer, Journal of Physics G: Nuclear and Particle Physics **49**, 010502 (2021).

[43] U. von Wimmersperg, G. Kernel, B. W. Allardyce, W. M. Mason, and N. W. Tanner, Physics Letters B **33**, 291 (1970).

[44] G. Baur, C. A. Bertulani, and H. Rebel, Nuclear Physics A **458**, 188 (1986).

[45] U. Friman-Gayer, HORST – Histogram Original Reconstruction Spectrum Tool, `https://github.com/u-eff-gee/Horst`, accessed: 2025-01-22.

[46] S. F. Biagi, Nucl. Inst. Meth A **421**, 234 (1999).

[47] C. R. Brune and D. B. Sayre, Nucl. Inst. Meth A **698**, 49 (2013).